# Correlative microscopy reveals abnormalities in type 1 diabetes

de Boer, Pascal

# Chapter 3

**Scanning EM of non-heavy metal stained biosamples: Large-field of view, high contrast and highly efficient immunolabeling**

Pascal de Boer[#], Jeroen Kuipers[#], Ben N.G. Giepmans

Department of Cell Biology, University Medical Center Groningen, Groningen, the Netherlands

[#] Denotes equal contribution

*Experimental Cell Research* (2015) 337(2): 202-207

**Abstract**

Scanning electron microscopy (SEM) is increasing its application in life sciences for electron density measurements of ultrathin sections. These are traditionally analyzed with transmission electron microscopy (TEM); by most labs, SEM analysis still is associated with surface imaging only. Here we report several advantages of SEM for thin sections over TEM, both for structural inspection, as well as analyzing immuno-targeted labels such as quantum dots (QDs) and gold, where we find that QD-labeling is ten times more efficient than gold-labeling. Furthermore, we find that omitting post-staining with uranyl and lead leads to QDs readily detectable over the ultrastructure, but under these conditions ultrastructural contrast was even almost invisible in TEM examination. Importantly, imaging in SEM with STEM detection leads to both outstanding QDs and ultrastructural contrast. STEM imaging is superior over back-scattered electron imaging of these non-contrasted samples, whereas secondary electron detection cannot be used at all. We conclude that examination of ultrathin sections by SEM, which may be immunolabeled with QDs, will allow rapid and straightforward analysis of large fields with more efficient labeling than can be achieved with immunogold. The large fields of view routinely achieved with SEM, but not with TEM, allows straightforward raw data sharing using virtual microscopy, also known as nanotomy when this concerns EM data in the life sciences.

## 1. Introduction

Conventional transmission electron microscopy (TEM), i.e. operation around 100 kV, has been the standard to analyze cross sections of biological samples for decades. The high energy of the electrons used in TEM enabled high resolution imaging. A drawback of TEM is the need for contrasting the sample with heavy metals, typically uranyl and lead, since the biological sample itself hardly scatters the high energy electrons resulting in low contrast. Scanning electron microscope (SEM) with a transmitted electron detector has been used for imaging ultrathin sections of tissues as an alternative for TEM. With the availability of field emission SEMs with high beam currents the image quality nowadays competes with that of TEM [1, 2]. The use of low energy scanning transmission EM (STEM) has also been shown to be useful in imaging of unstained biological samples [3]. The back scattered detector (BSD) in SEM is increasingly used for its ability to image ultrastructure of in plastic embedded tissue, so-called blockface, prior to sectioning, or for imaging of collected sections on a solid support [4]. This recently has been explored to generate 3D techniques like focused ion beam milling [5] or imaging of a large amount of serial sections [6, 7]. But the 3D techniques rely on the introduction of as much as possible heavy metals to prevent the samples from charging as well as for high yields of back-scattered electrons. Often multiple layers of osmium plus *en-bloc* staining with uranyl, lead and copper salts are used [8], giving almost binary images with outstanding membrane contrast. This is for example necessary for tracing neurons in consecutive images of 20 µm thick volumes [9]. The contrasting agents mask the intrinsic electron scattering differences of the biological sample itself. These properties can be useful to discriminate the different structures, for example the distinct secretory granules in pancreas. Another advantage of using unstained samples is that low contrast EM probes are more easily visible. Quantum dots (QDs) are not generally used in EM, probably because they are less electron dense than gold particles [10, 11]. However, they are advantageous over gold since the shelf-life is longer, penetrates better [11], can be used for correlated microscopy (reviewed in [12]) and label up to 10-fold more efficient than immunogold (below). We compared standard contrasting method with non-contrasted samples and immunolabeling followed by TEM and SEM acquisition with different detectors. STEM imaging of these non-contrasted QD labeled sections is superior over TEM imaging and is therefore a great

alternative, even more so when imaging large areas, or when other electron detectors or even optical detectors are used.

## 2. Materials and methods

### 2.1. Tissue and sample preparation

Rat pancreas was used as described before [13]. Briefly, fresh pancreas was cut into small pieces and fixed in 4% para-formaldehyde and 0.1% glutaraldehyde in 0.1 M sodiumcacodylate buffer, pH 7.4. 40 µm Vibratome sections were cut and selected for presence of islets of Langerhans. Those were postfixed with 1% osmiumtetroxide/1.5% potassiumferrocyanide in 0.1 M sodiumcacodylate, dehydrated through ethanol and embedded in EPON (Serva). Ultrathin sections (80 nm) were cut and collected on form-var coated nickel grids (electron microscopy sciences, Hatfield, Pennsylvania).

### 2.2. Post-embedding immunolabeling

Grids were incubated (room temperature) with tissue facing down on droplets on parafilm. First, samples were etched with 1% periodic acid (Merck, New Jersey) in milliQ water for 10 minutes to increase antigenicity. This was followed by 30 min blocking with 1% bovine serum albumin (BSA; Sanquin, The Netherlands) in tris-buffered saline (TBS), pH 7.4. Next, anti-insulin (guinea pig; 1:1000 in 1% BSA/TBS, Life Technologies) was incubated for 2 h, followed by four washes of 5 min with TBS and subsequent incubation for 1 h with biotinylated secondary antibody (donkey-anti-guinea pig; 1:400 in 1% BSA/TBS, Jackson Immunoresearch, UK) followed by four washes in TBS. Finally, streptavidin conjugated QD655 (1 µM; 1:1000 unless noted otherwise, in 1% BSA/TBS, Life Technologies) or 10 nm gold (various concentrations, BBI solutions, United Kingdom) were added for 1 h followed by four washes in TBS and two in 0.1 M sodiumcacodylate. Subsequently, samples were either post-stained with 2% uranyl-acetate in methanol and Reynold's lead-citrate or left untreated. Labeling efficiency was quantified by counting the number of particles (gold or QDs) per fifty insulin granules of a similar size with the counting tool in Photoshop (Adobe).

### 2.3. Transmission EM

Imaging of the samples was in a FEI CM100bio TEM at 80 KV equipped with a digital camera (Morada, OlympusSIS). The resolution of the camera was set on 3072×2304 pixels to match the resolution of the SEM.

### 2.4. Scanning (transmission) EM

If feasible, the same area recorded in the TEM was imaged in a Zeiss Supra55 SEM equipped with a 100 nano-Ampere anode. Because the magnification in SEM differs from the TEM, the SEM magnification is determined by the scanned area related to output on polaroid format, we adjusted magnification and rotation to match the field of view. STEM detection with a four quadrant STEM detector used in inverted darkfield mode, was done at 29 kV with 30 µm aperture at 3.5 mm working distance. BSD detection was done at 5 kV with 60 µm aperture at 6.5 mm working distance using high current mode. Secondary electron detection using the Everhart–Thornley detector or an inLens detector was done at 5 kV, 30 µm aperture at 3.5 mm working distance. All images were recorded at the same scan speed (cycle time 1.5 minute at 3072×2304 pixels). Contrast and brightness were set based on a live histogram. High resolution large-scale STEM images of approximately 40×50 µm at 2.5 nm pixel size were generated with the external scan generator ATLAS (Fibics, Canada), individual tiles were stitched in VE viewer (Fibics, Canada) and exported as a single tif file or an html file. All data is available through virtual microscopy or www.nanotomy.org.

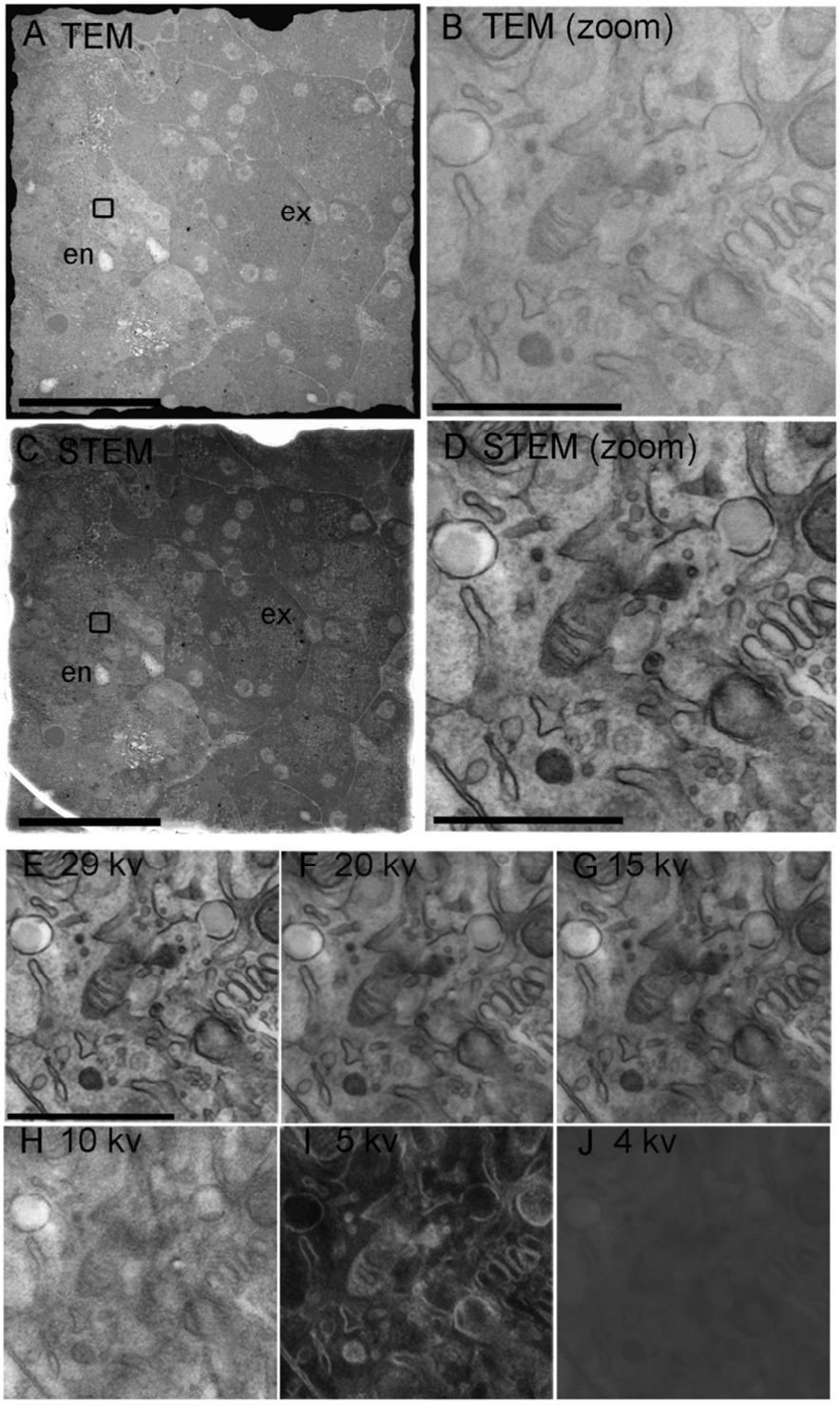


**Figure 1 | STEM imaging provides better tissue contrast in the absence of post-staining compared to TEM**. (A–D) TEM versus STEM imaging of an unstained rat pancreas 80 nm section containing both endocrine (en) and exocrine (ex) tissue. Compared to TEM (A and B), the STEM images (C and D) show more details and show better contrast. Bars in A and C 50 µm, B and D 1 µm. (E–J) Effect of different acceleration voltages on STEM image quality. 15 KV (G) gives still a good image, comparable to 29 KV (E). Going to 10 KV (H) gives a strong reduction of both contrast and resolution. Going down to 5 KV (I) results in a revival of image resolution and contrast, but also an unexpected inversion of the contrast which is lost at 4 kV (J). Bars: 1 µm

## 3. Results

Image acquisition was first with TEM followed by SEM. In samples without heavy metal post-staining, it was practically impossible to localize the islet of Langerhans on the phosphorescence screen of the TEM, because of lack of contrast. Furthermore, this lack of contrast impeded sharp focusing. Only after taking a digital image and setting white point and block points in the live image histogram, resulting in a grey level distribution covering only 10% of the dynamic range, endocrine cells could be

recognized from exocrine tissue (Fig. 1A). The same area was recorded in the SEM with STEM detection. Tracing back the area during live scanning was easy because the contrast could be controlled to yield an image covering the full dynamic range of 8 bits 256 grey values (Fig. 1C and D). Since the better contrast in STEM can be explained to some extend by the lower energy of the electrons, lower acceleration voltages were applied (Fig. 1E–J). Going down to 15 kV the tissue contrast was comparable or maybe even a bit less than at 29 kV. The image was more noisy and fine details in the cytoplasm disappeared. Still the image quality was good enough to recognize details as mitochondrial cristae, endocytic vesicles and stacks of the Golgi apparatus. Applying 10 kV acceleration voltage lead to a sharp drop in image quality. Low contrast and high noise preclude recognition of the aforementioned subcellular details. Remarkably, at 5 kV image quality improved, but grey levels were inverted. Going down to 4 kV still yielded low contrast, which needed the maximal STEM detector gain. Using even lower acceleration voltages, no electrons passed through the section making it impossible to obtain a STEM image. In conclusion, standard analysis of non-contrasted ultrathin sections is best performed with STEM at relative high (29 kV in our case) acceleration voltage.

Since heavy metal contrasting is not necessary for STEM [3], nanoparticles with less electron density than gold, such as QDs [10], will have sufficient contrast compared to surrounding tissue. Indeed, QD655 is hardly visible in heavily contrasted samples on the insulin granules, both in TEM and STEM and can only be detected at high magnification (Fig. 2A–D). Omitting the traditional post-staining with uranyl/lead (U/Pb) leads to outstanding QD655 contrast (Fig. 2E and F), but ultrastructural contrast was low in TEM, in agreement with our previous results (Fig. 1). On the other hand, STEM imaging showed high QD655 contrast in combination with good ultrastructural context, even at low magnifications (Fig. 2G and H). Since BSD is more often used and more often available than STEM detection, we also compared BSD signal on the non-contrasted QD655 labeled sample, as well as secondary electron detection by both the InLens detector, and the Everhart–Thornley detector (Fig. S1). BSD detection using the U/Pb contrasted sample showed even less outstanding QD contrast compared to STEM, whereas on non-contrasted sample this was similar. However the images were more noisy and showed less details as can be seen for example by the mitochondrial cristae being not resolved where they are in the STEM image (Fig. S1F). Secondary electron detection with the in lens detector gave similar pattern but with much less tissue contrast. The conventional SE2 detection with a Everhart–Thornley detector showed even less contrast and when omitting U/Pb no image was obtained (Fig. S1G and H). We conclude STEM detection is the best choice for imaging non-contrasted samples. Thus, in general tissue contrast was better with U/Pb post-staining, but masks the QDs and omitting U/Pb staining lead to improved QD contrast. Immunogold labeling is better identifiable than QDs, probably because of higher electron density. However QDs are advantageous as they are more stable during storage, are also well observable when U/Pb contrasting is omitted (see above) but also penetrate better [10]. Therefore, we compared labeling efficiency of QDs (QD655, Fig. 3A) and 10 nm gold (Fig. 3B). A striking ~10 times higher labeling efficiency was observed with QD655 compared to 10 nm gold (Fig. 3C). Using different concentrations of QD or gold reagents similar labeling densities were quantified, so excluding a concentration effect.

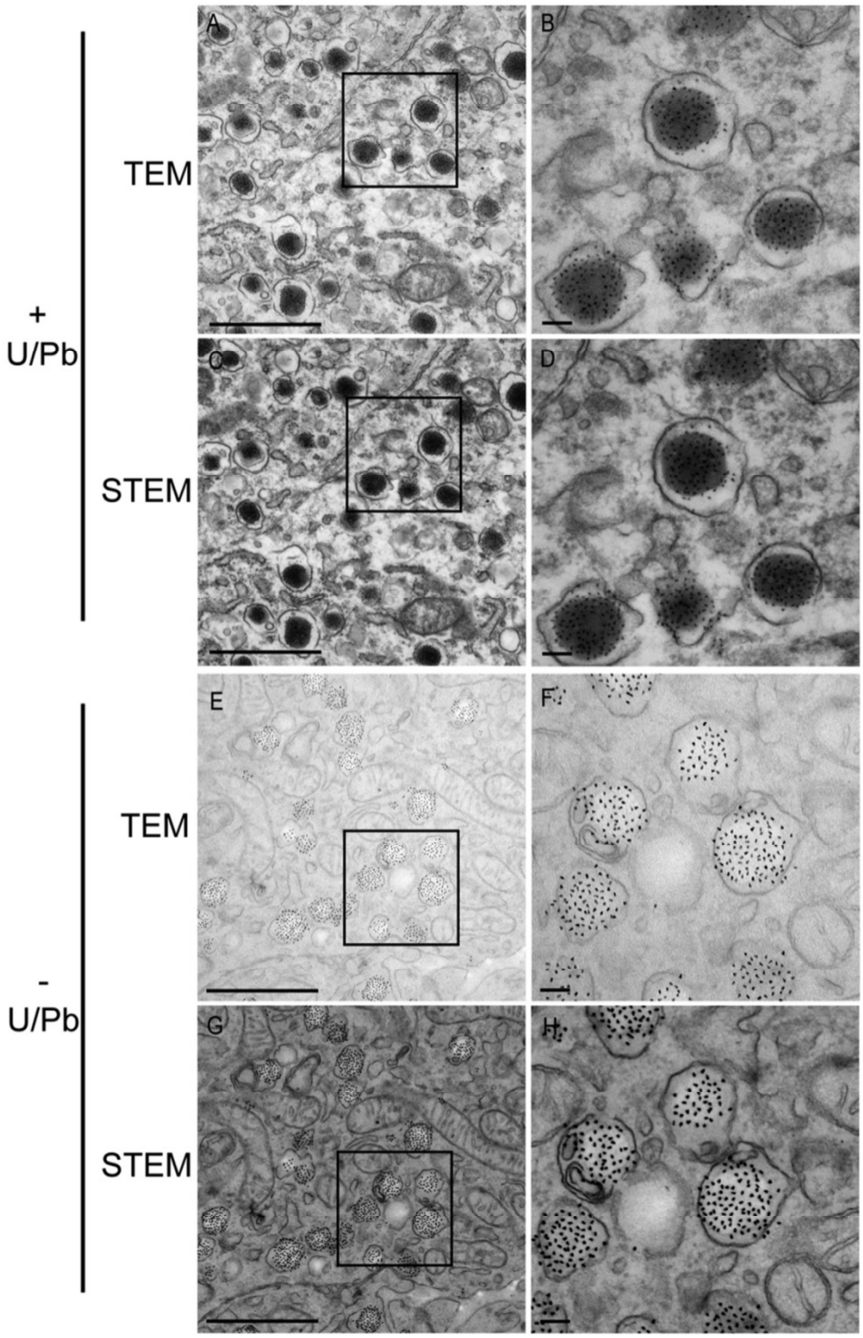


**Figure 2 | Detection of QD655 with STEM is superior over TEM in the absence of U/Pb contrasting**. (A–D) With uranyl and lead post-staining QDs are barely visible on insulin granules of rat pancreas, without differences between TEM and STEM. (E–H) Omitting U/Pb gives outstanding QD655 contrast, but with TEM the contrast of the tissue is very low (E and F). In STEM both the QD655 and the tissue show good contrast (G and H). Bars 1 µm (left panels) or 0.1 µm (right panels).

## 4. Discussion

Scanning EM imaging of biological samples is getting more popular for imaging electron density instead of surface information. Beneficially, SEM allows relative straightforward 3D analysis by serial section array tomography, focused ion beam milling or even serial blockface imaging with a microtome inside the SEM (for recent reviews see [14, 15]). These techniques in general use BSD, which requires extensive heavy metal staining with multiple layers of osmium and *en-bloc* uranyl and lead staining, all for enhancing conductivity and contrast [8]. Using the transmission detector, STEM, for ultrathin sections single-frame images of more than sixty times the size of TEM can be acquired in

the SEM [1]. Adding automated STEM mosaic acquisition and stitching allows imaging of extreme large areas at high resolution [1, 2, 16]. We find that STEM acquisition of these non-contrasted samples gives higher contrast than TEM imaging, with the added benefit that intrinsic differences in electron density within biological samples can be better observed (Fig. 3C). Omitting heavy metal post-staining of biological samples in routine TEM is rarely done [3], majorly because of the lack of contrast (Fig. 2A and B; mind that on the phosphorescence screen samples were almost undetectable). However, uranyl/lead post-staining of samples obscure signals of nanoparticles such as QDs. Without U/Pb, the contrast seen with both TEM and S(T)EM mostly comes from membranes due to osmium fixation, with these membranes much more pronounced in S(T)EM (Fig. 1). It should be noted that contrast formation in STEM, based on forward scattering, is widely different from that in TEM which uses phase contrast. Nevertheless, we observe that under the typical imaging conditions used here STEM holds a benefit for unstained sections over TEM. For STEM, the number of scattering events within the 80 nm section determines the contrast. Above 15 kV, this apparently stays constant (Fig. 1B), which is not unreasonable given that the total electron interaction volume at these energies would be a micrometer or larger. Surprisingly, a STEM image with an acceleration voltage as low as 5 kV could be obtained using an unstained 80 nm section showing more details and less noise than at 10 kV. Here, the image contrast was inverted with membranes being white instead of black. This might because below 5 kV the entire interaction volume falls within the section and no electrons penetrate. 5 kV Maybe the point where osmium-rich parts block all electrons, but through carbon forward-scattered electrons can still escape, leading to a black–white contrast. At 10 kV almost all electrons might undergo multiple scattering events and the signal becomes blurred. We note that, in contrast to STEM, BSD typically uses lower energy (<5 kV) electrons. With a circular BSD detector, contrast and resolution is less in BSD than STEM detection (Fig. S1E and F), but note that this may be different on microscopes with more elaborate BSD detector configurations or when imaging under immersion or stage-bias.

The label stands out in unstained samples, because differences in electron scattering between the label and surrounding tissue is higher. Indeed QDs, which are less electron dense than immunogold, only are easily detectable in the absence of U/Pb, with a superior contextual contrast with STEM over TEM (Fig. 2). Moreover, the QD-labeling beats conventional immunogold-labeling by a factor of 10 in these conditions (Fig. 3), which also accounts for other epitopes (data not shown). Quantification of EM data is often a hurdle as single snapshots by TEM at a high resolution are limited to a small field of view [17]. Automated large-scale 2D imaging with STEM has shown its value before for quantification [18]. Additional to efficient quantification, large-scale EM is less biased [19] and enables the observation of rare or interesting events unrelated to the research question as it does not depend on the selection of small regions of interest. These benefits are best harvested when sharing data open access via virtual microscopy or nanotomy. Interpretation of our data is open to all other, non-selected areas (www.nanotomy.org).

In conclusion, imaging of non-contrasted samples to observe intrinsic contrast differences or label identification, can best be performed in STEM. In addition, the efficient QDs labeling opens new avenues for successful postembedding labeling where gold labeling failed. STEM imaging also has the big advantage that large areas can be scanned as can be seen in the online datasets, typically resulting in data of approximately 40×50 $\mu m^2$ with a 2.5 nm pixel resolution, whereas digital TEM provides a field of view of just a few µm square at this resolution. Large area recordings facilitate data recognition of rare events and/or labeling more easy, quantification, and diminishes bias during selection of region of interest.

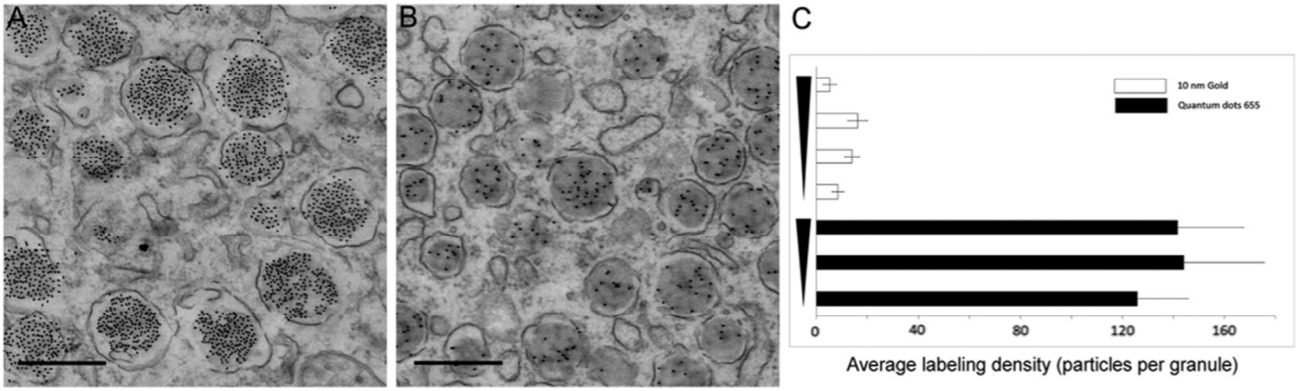


**Figure 3 | QD655 labeling is more efficient than 10 nm immunogold. Post-embedding immunolabeling for insulin with QD655** (A) or 10 nm gold (B) detection on rat pancreas. QD655 gives ten times more label density of insulin granules of similar sizes compared to 10 nm gold without the influence of label concentration (C). Different concentrations tested, from top to bottom are streptavidin QD655 1:500 (1), 1:1000 (2) and 1:2000 (3), and streptavidin 10 nm gold 1:50 (1), 1:100 (2), 1:200 (3) and 1:500 (4). Large-scale datasets per label concentration are provided online. Scale bars are 200 nm

## Acknowledgments

We thank our departmental members and Jacob P. Hoogenboom (Delft University of Technology, The Netherlands) for feedback and acknowledge financial support from the Netherlands Organization for Scientific Research (ZonMW91111006; “Microscopy Valley” STW12718; NWO175-010-2009-023).

## References

[1] M. Kuwajima, J.M. Mendenhall, L.F. Lindsey, K.M. Harris, Automated transmission-mode scanning electron microscopy (tSEM) for large volume analysis at nanoscale resolution, PLoS One. 8 (2013) e59573.

[2] M. Kuwajima, J.M. Mendenhall, K.M. Harris, Large-volume reconstruction of brain tissue from high-resolution serial section images acquired by SEM-based scanning transmission electron microscopy, Methods Mol. Biol. 950 (2013) 253-273.

[3] A. Takaoka, T. Hasegawa, Observations of unstained biological specimens using a low-energy, high-resolution STEM, J. Electron. Microsc. (Tokyo). 55 (2006) 157-163.

[4] K.L. Briggman, D.D. Bock, Volume electron microscopy for neuronal circuit reconstruction, Curr. Opin. Neurobiol. 22 (2012) 154-161.

[5] G. Knott, H. Marchman, D. Wall, B. Lich, Serial section scanning electron microscopy of adult brain tissue using focused ion beam milling, J. Neurosci. 28 (2008) 2959-2964.

[6] H. Horstmann, C. Korber, K. Satzler, D. Aydin, T. Kuner, Serial section scanning electron microscopy (S3EM) on silicon wafers for ultra-structural volume imaging of cells and tissues, PLoS One. 7 (2012) e35172.

[7] M. Reichelt, L. Joubert, J. Perrino, A.L. Koh, I. Phanwar, A.M. Arvin, 3D reconstruction of VZV infected cell nuclei and PML nuclear cages by serial section array scanning electron microscopy and electron tomography, PLoS Pathog. 8 (2012) e1002740.

[8] J.C. Tapia, N. Kasthuri, K.J. Hayworth, R. Schalek, J.W. Lichtman, S.J. Smith, J. Buchanan, High-contrast en bloc staining of neuronal tissue for field emission scanning electron microscopy, Nat. Protoc. 7 (2012) 193-206.

[9] K.J. Hayworth, C.S. Xu, Z. Lu, G.W. Knott, R.D. Fetter, J.C. Tapia, J.W. Lichtman, H.F. Hess, Ultrastructurally smooth thick partitioning and volume stitching for large-scale connectomics, Nat. Methods. 12 (2015) 319-322.

[10] B.N. Giepmans, T.J. Deerinck, B.L. Smarr, Y.Z. Jones, M.H. Ellisman, Correlated light and electron microscopic

imaging of multiple endogenous proteins using quantum dots, Nat Methods. 2 (2005) 743-9.

[11] R. Nisman, G. Dellaire, Y. Ren, R. Li, D.P. Bazett-Jones, Application of quantum dots as probes for correlative fluorescence, conventional, and energy-filtered transmission electron microscopy, J. Histochem. Cytochem. 52 (2004) 13-18.

[12] P. de Boer, J.P. Hoogenboom, B.N. Giepmans, Correlated light and electron microscopy: Ultrastructure lights up! Nat. Methods. 12 (2015) 503-513.

[13] R.B. Ravelli, R.D. Kalicharan, M.C. Avramut, K.A. Sjollema, J.W. Pronk, F. Dijk, A.J. Koster, J.T. Visser, F.G. Faas, B.N. Giepmans, Destruction of tissue, cells and organelles in type 1 diabetic rats presented at macromolecular resolution, Sci. Rep. 3 (2013) 1804.

[14] L. Hughes, C. Hawes, S. Monteith, S. Vaughan, Serial block face scanning electron microscopy--the future of cell ultrastructure imaging, Protoplasma. 251 (2014) 395-401.

[15] C.J. Peddie, L.M. Collinson, Exploring the third dimension: Volume electron microscopy comes of age, Micron. 61 (2014) 9-19.

[16] E. Sokol, D. Kramer, G.F. Diercks, J. Kuipers, M.F. Jonkman, H.H. Pas, B.N. Giepmans, Large-scale electron microscopy maps of patient skin and mucosa provide insight into pathogenesis of blistering diseases, J. Invest. Dermatol. 135 (2015) 1763-1770.

[17] T.M. Mayhew, Quantitative immunocytochemistry at the ultrastructural level: A stereology-based approach to molecular nanomorphomics, Cell Tissue Res. 360 (2015) 43-59.

[18] J. Kuipers, T.J. van Ham, R.D. Kalicharan, A. Veenstra-Algra, K.A. Sjollema, F. Dijk, U. Schnell, B.N.G. Giepmans, FLIPPER, a combinatorial probe for quantitative correlated live imaging and electron microscopy, Cell & Tissue Research. 360 (2015) 61-70.

[19] F.G. Faas, M.C. Avramut, B. M van den Berg, A.M. Mommaas, A.J. Koster, R.B. Ravelli, Virtual nanoscopy: Generation of ultra-large high resolution electron microscopy maps, J. Cell Biol. 198 (2012) 457-469.

**Supplementary information**

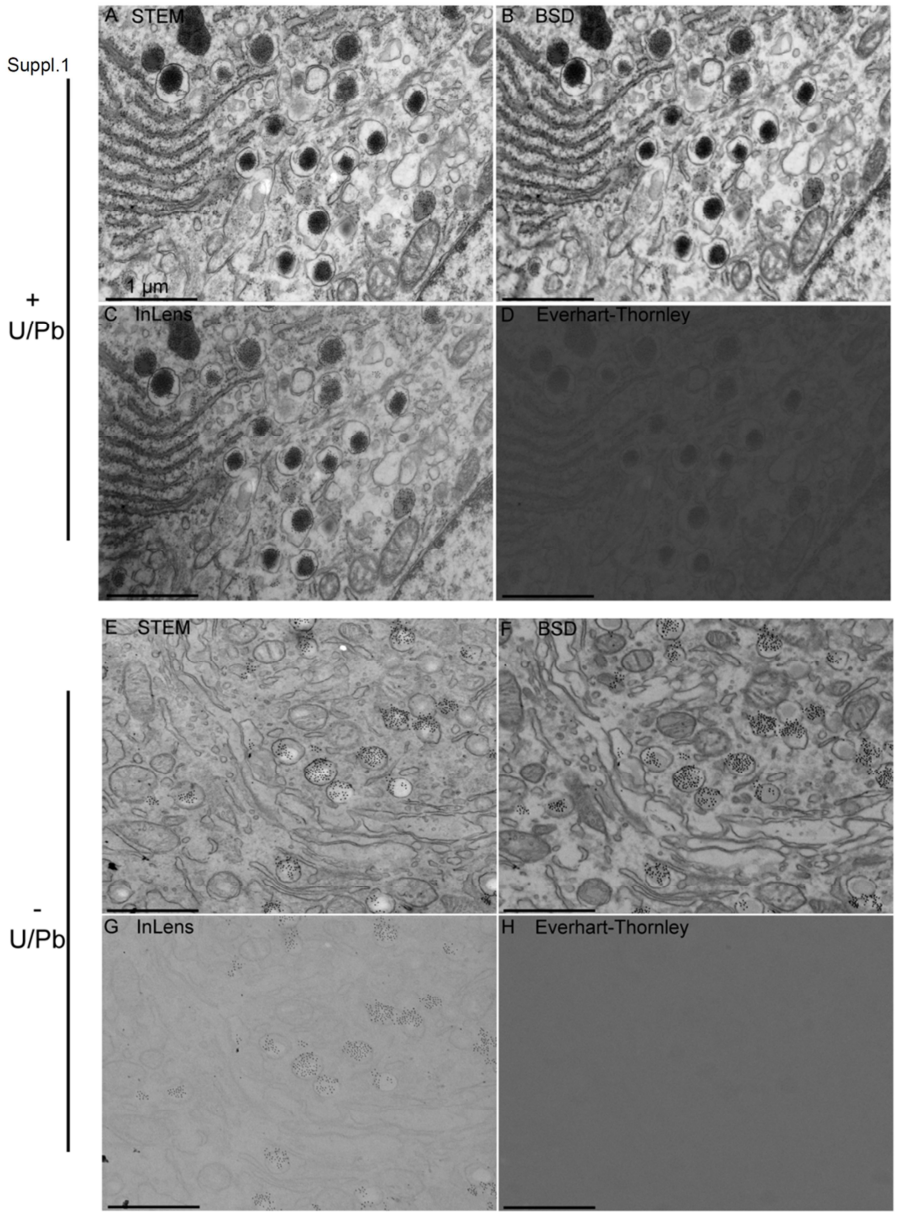


**Supplementary figure 1 | STEM detection is superior for imaging of non-contrasted samples compared to other available SEM detectors**. Different SEM detectors imaging of U/Pb contrasted (A–D) and non-contrasted (E–H) samples. U/Pb provides good tissue contrast when STEM (A), BSD (B) and InLens (C) detection is used, but with a slightly lower resolution compared to STEM (eg. mitochondrial cristae). However, QDs are again masked with BSD and InLens detection in the presence of U/Pb (B and C) similar to STEM detection (A). SE2 detection with the Everhart-Thornley detector gives very poor contrast (D). In non-contrasted samples, QDs also stand out when imaged with BSD (F) and InLens detection of secondary electrons (G). However, tissue contrast and resolution with BSD (F) is less compared with STEM (E) and no tissue is observed with InLens (G). Note that mitochondrial cristae are not observed with BSD at this magnification (F). SE2 detection with the Everhart-Thornley detector gives no tissue or QD contrast at all (H). The InLens and SE2 images (C and D, G and H) are displayed here with inverted contrast. Scale bars are 1 µm.